Out-of-plane high-density piezoresistive silicon microwire/p–n diode array for force- and temperature-sensitive artificial whisker sensors

2011 J. Micromech. Microeng. 21 035007

(http://iopscience.iop.org/0960-1317/21/3/035007)

J. Micromech. Microeng. **21** (2011) 035007 (7pp) doi:10.1088/0960-1317/21/3/035007

Out-of-plane high-density piezoresistive silicon microwire/p–n diode array for force- and temperature-sensitive artificial whisker sensors

Akihito Ikedo, Makoto Ishida and Takeshi Kawano

Department of Electrical and Electronic Information Engineering, Toyohashi University of Technology, 1-1 Hibarigaoka, Tempaku-cho, Toyohashi, Aichi 441-8580, Japan

E-mail: ikedo-a@int.ee.tut.ac.jp

Received 4 October 2010, in final form 21 December 2010
Published 3 February 2011
Online at stacks.iop.org/JMM/21/035007

Abstract

We propose an out-of-plane high-aspect-ratio 'whisker-like' microwire array sensor for use in multisite contact force and temperature detection with high spatial resolution. Although the wire element has two terminal electrodes, the device consists of force-sensitive wire arrays where one end of the wire is attached to the substrate and the other end is free to be touched. We fabricated a force-sensitive wire array based on p-type (p-) silicon with 3 μm diameter and 30 μm length (1 Ω cm) assembled over an n-type (n-) silicon substrate (3–6 Ω cm), which resulted in a p-silicon wire/p–n diode system array. Due to the piezoresistance effect of the p-silicon wire, the electrical conductance changes upon contact of an individual wire with an object. The shift in the rectifying current–voltage (I–V) curves of the embedded p–n diode depends on the temperature through the silicon wire. Thus, the same alignment can be used as a force sensor and a temperature sensor. Both force- and temperature-sensitive microwire sensor arrays with a small detection area (~20 μm^2) and high spatial resolution (~100 μm in pitch) have potential in numerous applications, including artificial electronic fingertips in a robot hand/prosthetics, multisite sensing of contact force, shear force, surface roughness and slip, and local temperature sensing capabilities.

S Online supplementary data available from stacks.iop.org/JMM/21/035007/mmedia

(Some figures in this article are in colour only in the electronic version)

1. Introduction

Because biological whiskers have an exquisite tactile sensing ability, investigations of artificial whisker sensors strive to develop more force sensitivity and functions suitable for touching and analyzing objects. Centimeter-order biomimetic whisker-type tactile sensors have been developed for displaying the surface shapes of contact objects [1, 2]. Due to advances in micro/nanofabrication technology, 'planar-type' force-sensitive micro/nano-scale sensors have been realized utilizing either the piezoresistance effect of semiconducting materials or the piezojunction effect of p–n junctions [3–7]. However, conventional etching-based processes, such as deep reactive ion etching (DRIE), have limited the fabrication of out-of-plane high-aspect-ratio 'whisker-type' force-sensitive micro/nano-scale diameter wires. Although the vapor–liquid–solid (VLS) method [8] enables the production of out-of-plane semiconducting micro/nanowires, the electrical interconnection to an individual wire tip to utilize the piezoresistance effect of the wire is problematic. Additionally, the local temperature-sensing capability of the whisker-type sensor is another powerful functionality in thermal material analysis [9].

Here we fabricate an out-of-plane, high-density force- and temperature-sensitive artificial microscale whisker array sensor. Additionally, we discuss batch fabrication of the

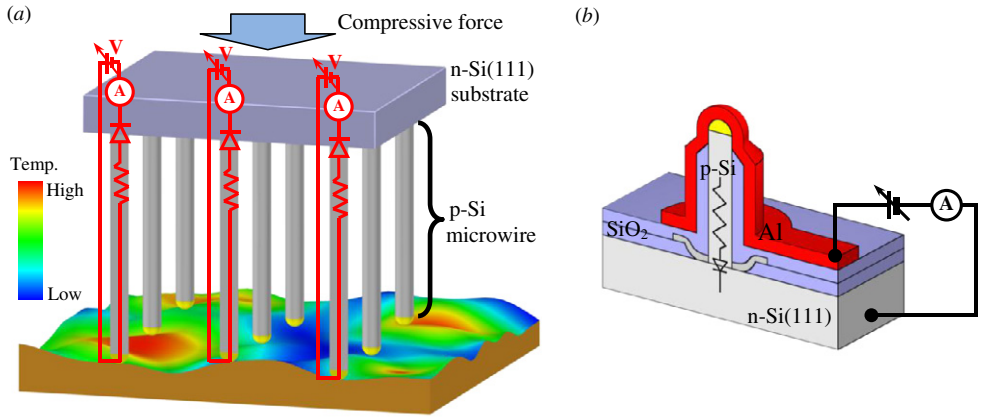

Figure 1. Out-of-plane silicon microwire-based artificial whisker array sensor by selective VLS growth of p-silicon on an n-silicon substrate. (*a*) Schematic illustration of an artificial whisker array and (*b*) cross-sectional device image of an individual whisker sensor element consisting of a piezoresistive p-silicon VLS-microwire assembled over an n-silicon substrate, realizing a p-silicon wire/p–n diode system. Using the same sensing alignment, the piezoresistive silicon microwire and the embedded p–n diode can be utilized in force and temperature sensing, respectively.

p-silicon microwire/p–n diode arrays and the characterization of the piezoresistance effect in the p-silicon microwire. Moreover, we report the temperature-sensing capability of an embedded p–n diode through the microwire for force- and temperature-sensitive microscale artificial whisker sensors.

This sensor is based on vertically assembled piezoresistive p-type (p-) silicon microwires on an n-type (n-) silicon substrate by utilizing gold (Au)-catalyzed selective VLS growth of silicon (figure 1). VLS growth is advantageous for realizing an artificial whisker sensor because the diameter and position of the silicon wire can be precisely defined by integrated-circuit (IC) lithography-based patterning of the catalytic Au. This precision results in a high-density wire array and various lengths of out-of-plane wires can be controlled on the micro to millimeter scale [8]. A p-silicon wire with a high longitudinal piezoresistance coefficient [10] has been realized by *in situ* doping VLS growth technology [11], and a temperature-sensitive p–n diode system can be embedded by simply utilizing n-silicon as the platform substrate. Additionally, we have demonstrated an IC-compatible VLS growth process [12, 13], which promises further on-chip integrations for detection circuitry and signal processors for whisker sensors.

2. Fabrication processes

Based on a reported higher longitudinal piezoresistance coefficient value of $\sim 93.5 \times 10^{-11}$ Pa^{-1} for ⟨1 1 1⟩ p-silicon (bulk) compared to those for other silicon types (e.g. -7.5×10^{-11} Pa^{-1} for ⟨1 1 1⟩ n-silicon (bulk)) [10, 14], we designed a piezoresistive microwire using VLS-grown ⟨1 1 1⟩ p-silicon (figure 2). We began with an n-silicon (1 1 1) substrate (resistivity 3–6 Ω cm) with a diameter and length of 3 and 30 μm, respectively, as well as p-silicon wire arrays, which were constructed by VLS growth using a Si_2H_6–B_2H_6 mixture gas at 0.6 Pa and 700 °C (figures 2(*a*) and (*b*)). Herein we used a controlled B_2H_6 concentration of ∼8000 ppm, which gave a p-silicon wire with a resistivity of 1 Ω cm [15]. For the electrical insulation of the conductive wire, a 600 nm thick silicon dioxide (SiO_2) layer was deposited by plasma enhanced chemical vapor deposition (PE-CVD) (figure 2(*c*)), and only the wire-tip section was subsequently exposed (figure 2(*d*)). The electrical interconnection of a 500 nm thick aluminum (Al) layer was formed over each wire by sputtering and lithography (figure 2(*e*)). To completely cover the wire, we then spray-coated a uniform photoresist (>2 μm), which was subsequently exposed via a projection printing technique without mechanically breaking the wires. Figures 2(*f*) and (*g*) show the scanning electron microscope (SEM) images of the silicon wire tip after SiO_2 etching and the subsequent Al deposition, respectively, and show a completed tip contact with an Al layer. Figures 2(*h*) and (*i*) show the SEM images of an as-VLS-grown silicon wire and the process completed wire, respectively, while figure 2(*j*) shows a fabricated 3 × 3 silicon microwire senor array with site spacings of 100 μm.

3. Experimental results and discussion

3.1. Force sensitivity of p-silicon wire

To characterize the piezoresistance effect of an individual p-silicon wire, we used a tungsten (W) needle with a tip measuring 5 μm in diameter and 4 cm in length affixed to the tip of a plastic bar (5 mm in diameter and 10 cm in length). The W needle could be precisely moved utilizing a manipulator control system with a 0.1 μm displacement resolution (figure 3(*a*)). Figure 3(*b*) shows the current–voltage (*I*–*V*) characteristics of a single p-silicon wire/p–n diode measured in standard atmosphere at room temperature (RT) while the silicon wire was compressed by the W needle.

Due to the embedded p–n diode at the p-silicon wire base, the *I*–*V* characteristics without wire compression exhibited rectifying behavior with a threshold voltage of +0.4 V. Figure 3(*c*) shows the *I*–*V* curves measured at 3.8–4.0 V, and clearly indicates that forward currents

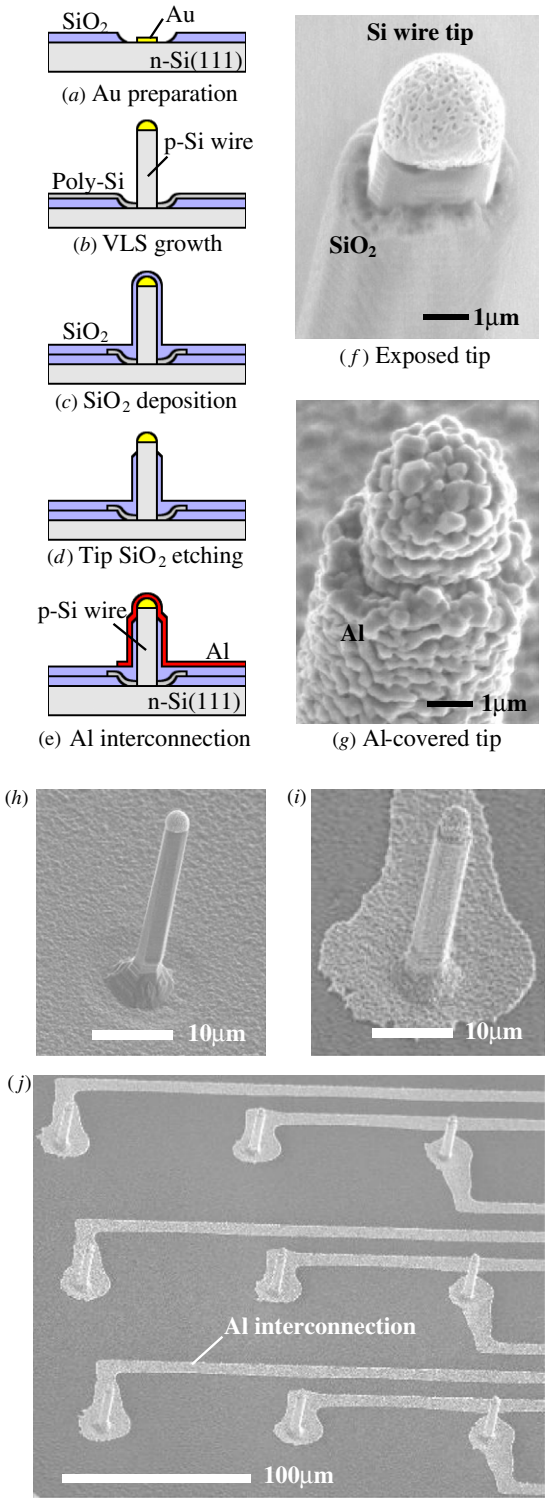

Figure 2. Process sequence and SEM images of the device. (*a*) Substrate preparation (n-silicon) with catalytic Au particles for VLS growth of a silicon wire, (*b*) VLS growth of a p-silicon wire using a Si_2H_6–B_2H_6 gas mixture (0.6 Pa, 700 °C), (*c*) electrical insulation of the wire by PE-CVD of SiO_2, (*d*) tip exposure, and (*e*) device completion after tip metallization (Al). (*f*), (*g*) SEM images of the wire-tip exposure and metallization, respectively. (*h*) As-VLS grown p-silicon wire measuring 3 μm in diameter and 30 μm in length, and (*i*) process completed wire. (*j*) Fabricated 3 × 3 silicon microwire array (site spacing = 100 μm).

progressed upon increasing the compressive force due to the piezoresistance effect in the p-silicon wire [3]. It should be noted that compressive-force-dependent reverse currents were also observed (figure 3(*b*)). Unfortunately, the large reverse current was due to the current through the leakage pass of the polycrystalline silicon layer system (p-type, ∼1 μm thick), which formed over the n-silicon region during the Si_2H_6 gas source-based VLS growth. Hence, process improvements are required in future fabrications [16] (see figure S1 in supplementary data available from stacks.iop.org/JMM/21/035007/mmedia). Figure 3(*d*) shows the compressive-force-dependent electrical resistance of the wire where the *x*-axis indicates the displacement of the plastic bar root, but not the exact displacement of the shrunken silicon wire. We hypothesized that both the plastic bar and W needle will be bent. The forward and reverse resistance values were taken under biases of 2 to 4 V and −10 to −8 V, respectively. In forward biases, a 15% change in resistance was observed, whereas the reverse biases exhibited a 9% change in resistance.

The manipulation system precisely controlled the position of the W needle. However, the manipulation system requires the force measurement system to quantitatively display the amount of applied force during the measurement. Before employing this device, a force measuring manipulation system can be used to calibrate the sensor. Herein we assumed that the downward W needle applied a uniaxial stress to the wire element, and the electric field and current were along the same silicon wire direction. With these assumptions, the stress applied to the silicon wire can be given by the resistivity difference of the p-silicon wire under the forward biases:

$$\sigma = \frac{\Delta\rho/\rho}{\Pi_{l\langle 1\,1\,1\rangle}}, \tag{1}$$

where ρ and $\Delta\rho$ are the resistivity under zero stress and the variation in the resistivity with stress, respectively, σ is the stress of the p-silicon wire, and $\Pi_{l\langle 111\rangle}$ is the longitudinal piezoresistance coefficient. To obtain the piezoresistance coefficient of a fabricated silicon wire, both changes in the resistivity and stress of the silicon wire are required (equation (1)). Although a W needle with a force measurement system is used, obtaining just the stress of the core silicon wire remains problematic due to the SiO_2/Al films around the core silicon wire. However, the piezoresistance coefficient of a silicon wire with a diameter greater than 100 nm does not differ from the bulk-Si piezoresistance coefficient [14]. Based on this understanding, the reported piezoresistance coefficient (93.5 × 10^{-11} Pa^{-1} for ⟨1 1 1⟩ bulk p-silicon) [10, 14] was used for the fabricated silicon microwire, and the applied maximum stress to the wire in this measurement should be −160 MPa (compressive stress) where the stress value corresponds to ∼0.1% strain in silicon [17] and ∼30 nm shrinkage for a 30 μm long silicon wire. For the change in resistivity $\Delta\rho/\rho$, we used the 15% changed resistance (forward bias) in the calculation. With a maximum stress of −160 MPa and the wire structure, the calculated amount of the applied maximum compressive force was ∼2 mN (see figure S2 in supplementary data available from stacks.iop.org/JMM/21/035007/mmedia).

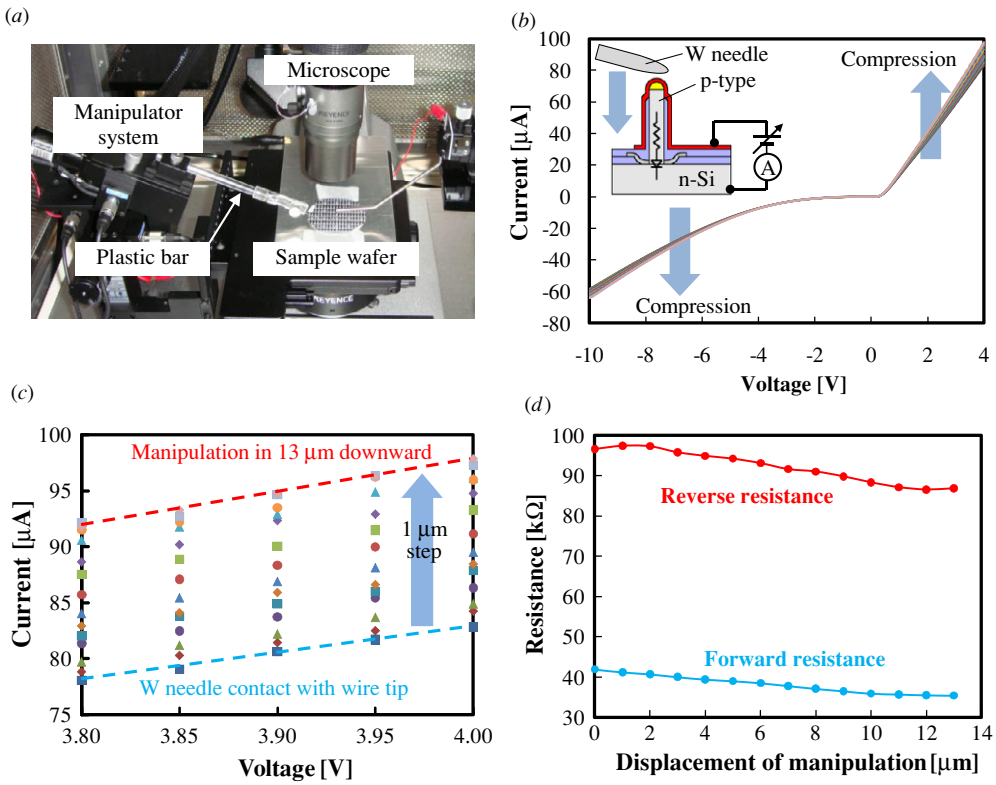

Figure 3. Force sensing via an individual piezoresistive p-silicon microwire. (*a*) Optical image of the experimental setup. Compressive force is applied to a silicon microwire using a W needle with a 5 μm tip diameter mounted on the micromanipulator system. (*b*) Current–voltage (*I–V*) characteristics of the p-silicon microwire/p–n diode as a function of compressive force. The arrowhead direction indicates an increase in the applied compressive force. (*c*) Fourteen *I–V* curves from the same wire element with forces ranging from zero to the maximum measured force. (*d*) Electrical resistance changes associated with wire compression under forward (♦) and reverse (■) biases. 'Displacement of manipulation' (*x*-axis) in the graph means the displacement of the plastic bar root, that is, where the plastic bar and W needle should bend.

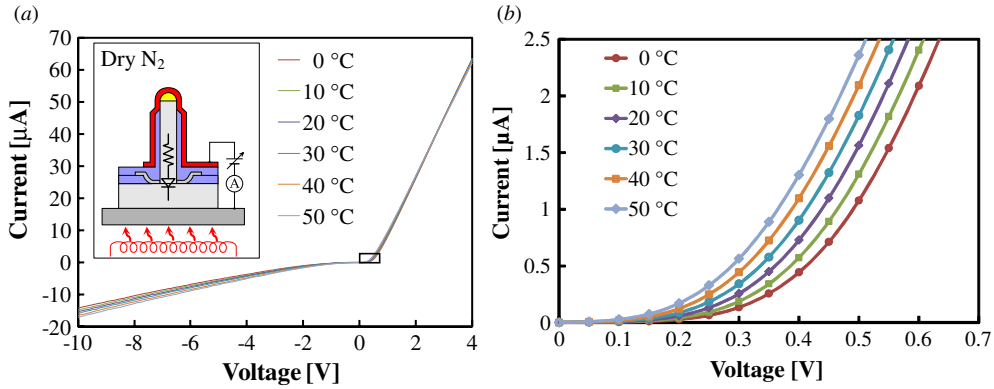

Figure 4. Temperature sensitivity of the embedded p–n diode. (*a*) *I–V* characteristics of an individual p-silicon wire/p–n diode system as a function of the device temperature (0–50 °C, 10 °C steps). The device temperature is varied by utilizing a temperature controllable stage. (*b*) *I–V* curve shifts of the wire/p–n diode observed at forward biases of 0 to 0.7 V due to a decrease in the temperature-induced built-in potential of the p–n diode. The temperature sensitivity of the embedded p–n diode is -2.3 mV °C^{-1} at 0.1 μA. All measurements are carried out in a dry nitrogen atmosphere.

3.2. Temperature sensitivity of the embedded p–n diode

With the VLS growth of p-silicon over an n-silicon substrate, the p–n diode system was simply embedded at each wire base, and served as a temperature sensor using the same sensing alignment as the force-sensing microwire. To sense temperature through silicon microwires, the temperature sensitivity of the embedded p–n diode must initially be characterized. A completed sensor device, which consisted of silicon microwire/p–n diode arrays, was placed on a temperature controllable stage (figure 4(*a*), inset image). All measurements were carried out in a dry nitrogen atmosphere. Figure 4(*a*) shows the measured *I–V* characteristics of an individual p-silicon wire/p–n diode system when the device temperature was varied from 0 to 50 °C in 10 °C increments. Due to the decrease in the built-in potential of the

p–n diode associated with the increased temperature [18], the rectifying *I–V* curves of the p-silicon wire/p–n diode negatively shifted, but the series resistance of the p-silicon wire increased due to the enhanced lattice scattering in the silicon wire (see figure S3 in supplementary data available from stacks.iop.org/JMM/21/035007/mmedia).

Figure 4(*b*) shows the temperature-dependent *I–V* curves of the wire/p–n diode measured at forward biases of 0 to 0.7 V. At forward biases between 0.1 and 0.25 V, the forward current was mainly dominated by the characteristics of the p–n diode (see figure S4 in supplementary data available from stacks.iop.org/JMM/21/035007/mmedia; the resistance of a p-silicon wire is ∼50 kΩ). Consequently, the temperature sensitivity of the embedded p–n diode was −2.3 mV °C^{-1} at 0.1 μA, which agrees well with that of reported silicon p–n diodes (−1 to −3 mV °C^{-1}) [19]. In addition, the measured temperature sensitivity of the p–n diode could be used in the temperature compensation of the series resistance of a p-silicon wire (see figure S3 in supplementary data available from stacks.iop.org/JMM/21/035007/mmedia).

3.3. Temperature sensing of a microscale area

Based on the temperature sensitivity of the embedded p–n diode (−2.3 mV °C^{-1} at 0.1 μA), we performed temperature sensing of a microscale area through a p-silicon microwire. The microscale 'hot' object was a 1 μm tip diameter W needle attached to four heating resistors (overall resistance = 50 Ω) with a good thermal conductive glue of silver paste (figure 5(*a*)); these resistors and the W needle were electrically insulated. By applying 12.0 V to these resistors, the W needle was heated by Joule heating of these resistors, and 80 °C heating from RT was quantitatively confirmed by black marks on the needle by thermography (TH5100, NEC Avid Infrared Technologies Co., Ltd). The heated W needle was fixed to an electrically insulating and thermally stable bamboo chopstick, which was then mounted on the same manipulator system used in the aforementioned force-sensing experiment (figure 5(*a*)).

Using the hot W microneedle, microscale local temperature measurements through a p-silicon microwire were carried out in a dark shielded box. Herein we employed a sensing voltage range of 0.19 to 0.25 V, to eliminate the piezoresistance effect of the p-silicon wire on the measured *I–V* characteristics (the threshold voltage of the p–n diode is ∼+0.4 V). To confirm the effect of the W needle contact force, we measured the *I–V* characteristics of the p-silicon wire/p–n diode system prior to heating the W needle (RT-W needle) with and without the RT-W needle contact. Consequently, these two *I–V* curves exhibited a small change in the characteristics with a resistance of 636 kΩ, confirming that the W needle contact has a negligible contribution in this voltage range (figure 5(*b*)). Next, the RT-W needle was heated (12.0 V applied to the attached resistors), and the tip of the hot W needle was placed 5 μm above the tip of the silicon wire, resulting in a −3.0 mV shift of the *I–V* curve. The heating of the silicon wire/p–n system was due to heat transfer via the air surrounding the W needle.

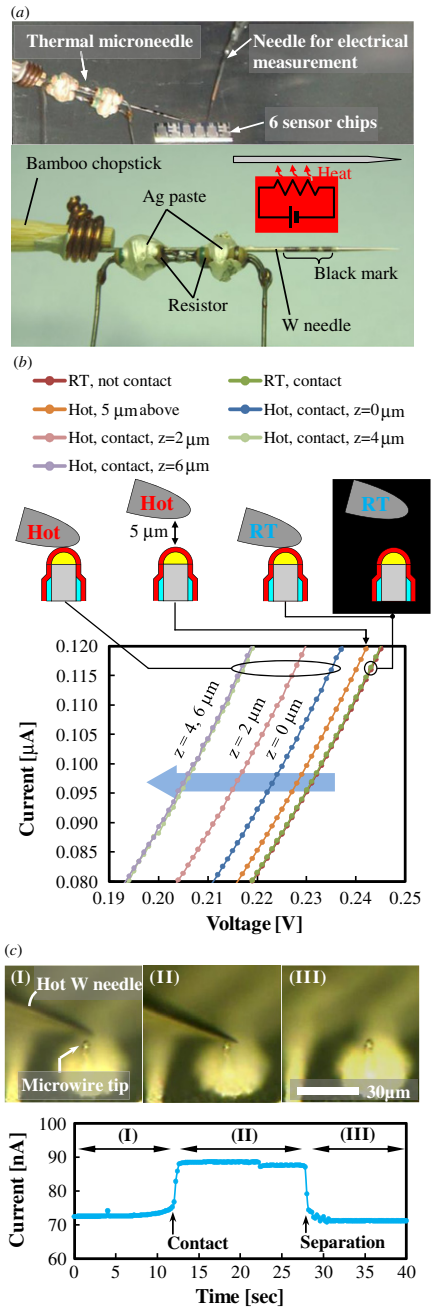

Figure 5. Local temperature sensing via an individual p-silicon microwire/p–n diode system and real-time temperature sensing. (*a*) Optical image of the experimental setup for the local temperature sensing utilizing a 'hot' W microneedle (tip diameter = 1 μm). Joule heating of the attached resistors heated the W needle (bottom image). (*b*) *I–V* characteristics of the p-silicon wire/p–n diode system: the RT-W needle contact (dark green), without the RT-W needle contact (red), hot W needle located 5 μm above the wire tip (orange), and the hot W needle contact with a manipulation height *z* = 0 (blue), 2 (pink), 4 (light green), and 6 μm (purple). For measurements with a 'hot' W needle, the needle is heated by applying 12.0 V to the resistors. (*c*) Real-time temperature sensing of the contact/separation of the 'hot' W needle via an individual p-silicon microwire/p–n diode system: before contact (I), during contact (II), and after separation of the 'hot' needle from the silicon wire tip (III), indicating a sub-second response speed. Microscopic observations of the contact/separation of the needle during real-time measurements employ a constant light condition.

Based on the measured sensitivity of the embedded p–n diode (figure 4(*b*)), the temperature at the wire-base p–n diode was increased by 1.3 °C. Subsequently, the hot W needle made contact with the silicon wire tip, resulting in a significant voltage shift of −7.9 mV, and 3.4 °C heating was expected (manipulation height z = 0 μm; see more details in supplementary data available from stacks.iop.org/JMM/21/035007/mmedia). Although the *I–V* curve shifted due to contact with the needle ($z = 0$ μm), the needle moved downward. When the hot W needle was moved further downward to $z = 2$ μm and $z = 4$ μm, the *I–V* curve shifted to −15.3 mV (expected heating of 6.7 °C) and −25.7 mV (expected heating of 11.2 °C), respectively. However, the *I–V* curve measured at $z = 6$ μm was almost the same as that of $z = 4$ μm.

The effect of the manipulation height (z = 0, 2, 4, and 6 μm) on the *I–V* curve is further discussed considering the impact of thermal contact resistance between the hot W needle tip and the silicon wire tip. Setting the manipulation height z to 0 or 2 μm, the heat conduction to the silicon wire/p–n diode might be limited by the thermal contact resistance between the W needle tip and the silicon wire tip. Increasing the manipulation height z, which moved the W needle further downward, shifted the *I–V* curves, suggesting a reduction in the thermal contact resistance and good heat conduction to the silicon wire. In contrast, for stronger contact forces with manipulation heights of $z = 4$ and 6 μm, characteristic shifts were no longer observed. This also suggests that the effect of thermal contact resistance becomes negligible because the good thermal contact as well as the heat conduction to the p–n diode through the silicon wire at manipulation heights $z = 4$ and 6 μm is limited by the thermal resistance of the silicon wire element.

3.4. Real-time temperature sensing

The silicon microwire-based temperature sensor should be advantageous for accurate temperature measurements due to the small temperature detection area and thermal material mappings with a high spatial resolution. Additionally, this sensor may offer a fast response time due to the small thermal capacity system of the microwire (silicon wire length = 30 μm, silicon wire diameter = 3 μm, dioxide thickness = 600 nm, aluminum thickness = 500 nm), as demonstrated by the real-time temperature measurement using the same hot W needle configuration (figure 5(*c*)) where a constant forward bias of 234 mV was applied to a p-silicon wire/p–n diode and forward current was measured in 0.2 s steps. Before the hot W needle made contact with the silicon wire (upper-left image in figure 5(*c*)), the measured current was 72.5 nA, but this suddenly jumped to 89 nA at the moment of contact (middle image in figure 5(*c*)). After separating the hot W needle and the silicon wire tip (upper-right image in figure 5(*c*)), the current decreased to 71.2 nA. Because the hot W needle was close to the silicon wire tip prior to the W needle contact, the heat conduction effect of the hot W needle caused the difference between the wire current before the contact (72.5 nA) and after the separation (71.2 nA) of the W needle. The measured response times for the contact and separation of the hot W needle were ∼0.8 and ∼0.6 s, respectively, demonstrating the temperature detection capability in a microscale area with a sub-second temporal resolution. Based on the designed sensor configuration and the demonstrated real-time measurements, the measured thermal response time was dominated by the large thermal capacity system of the silicon substrate, indicating that further higher thermal response times could be realized by utilizing a device substrate with smaller thermal capacitance characteristics. In addition, the thermal contact resistance between the hot W needle tip and the silicon wire tip contributed to the measured response time. The thermal contact resistance can be reduced by a silicon wire tip coated with highly thermal conductive liquid/glue [9].

4. Conclusion

In conclusion, we have developed force- and temperature-sensitive p-silicon microwire/p–n diode arrays by utilizing VLS growth. We confirmed the compression-induced changes in the electrical characteristics of an individual silicon microwire due to the piezoresistance effect of the p-silicon wire. Temperature-sensitive p–n diodes were successfully embedded in each force-sensitive silicon wire base using the VLS growth of p-silicon microwires over the n-silicon substrate, enabling a temperature sensor with the same alignment. Although we separately demonstrated the force- and temperature-sensing capabilities, the p-silicon microwire/p–n diode array sensor should be applicable to simultaneous force and temperature sensing with a high spatial resolution; thus, this sensor has potential in numerous applications, including artificial electronic fingertips of a robot hand/prosthetics for sense of touch and force/temperature mapping probe arrays to investigate small materials as well as biological soft samples.

Acknowledgments

The authors would like to thank Mitsuaki Ashiki for his assistance with the fabrication processes. This work was supported by a Grant-in-Aid for Scientific Research (S) by the Global COE Program ‘Frontiers of Intelligent Sensing’ and by Strategic Research Program for Brain Sciences (SRPBS) from the Ministry of Education, Culture, Sports, Science and Technology of Japan (MEXT).

References

[1] Solomon J H and Hartman M Z 2008 Artificial whiskers suitable for array implementation: accounting for lateral slip and surface friction *IEEE Trans. Robot.* **24** 1157–67
[2] Kim D and Möller R 2007 Biomimetic whiskers for shape recognition *Robot. Auton. Syst.* **55** 229–43
[3] Smith C S 1954 Piezoresistance effect in germanium and silicon *Phys. Rev* **94** 42–9
[4] Rindner W 1962 Resistance of elastically deformed shallow p–n junctions *J. Appl. Phys.* **33** 2479–80

[5] Tortonese M, Barrett R C and Quate C F 1993 Atomic resolution with an atomic force microscope using piezoresistive detection *Appl. Phys. Lett.* **62** 834–6
[6] Puers B, Reynaert L, Snoeys W and Sansen W 1988 A new uniaxial accelerometer in silicon based on the piezojunction effect *IEEE Trans. Electron Devices* **35** 764–70
[7] Creemer J F, Fruett F, Meijer G C M and French P J 2001 The piezojunction effect in silicon sensors and circuits and its relation to piezoresistance *IEEE Sensors J.* **1** 98–108
[8] Wagner R S and Ellis W C 1964 Vapor–liquid–solid mechanism of single crystal growth *Appl. Phys. Lett.* **4** 89–90
[9] Shi L, Plyasunov S, Bachtold A, McEuen P L and Majumdar A 2000 Scanning thermal microscopy of carbon nanotubes using batch-fabricated probes *Appl. Phys. Lett.* **77** 4295–7
[10] Kanda Y 1982 A graphical representation of the piezoresistance coefficients in silicon *IEEE Trans. Electron Devices* **29** 64–70
[11] Ikedo A, Kawashima T, Kawano T and Ishida M 2009 Vertically aligned silicon microwire arrays of various lengths by repeated selective vapor–liquid–solid growth of n-type silicon/n-type silicon *Appl. Phys. Lett.* **95** 033502
[12] Kawano T, Kato Y, Tani Y, Takao H, Sawada K and Ishida M 2004 Selective vapor–liquid–solid epitaxial growth of micro-Si probe electrode arrays with on-chip MOSFETs on Si (1 1 1) substrates *IEEE Trans. Electron Devices* **51** 415–20
[13] Takei K, Kawashima T, Kawano T, Takao H, Sawada K and Ishida M 2008 Integration of out-of-plane silicon dioxide microtubes, silicon microprobes and on-chip NMOSFETs by selective vapor–liquid–solid growth *J. Micromech. Microeng.* **18** 035033
[14] He R and Yang P 2006 Giant piezoresistance effect in silicon nanowires *Nat. Nanotechnol.* **1** 42–6
[15] Islam M S, Ishino H, Kawano T, Takao H, Sawada K and Ishida M 2005 Realization of *in situ* doped n-type and p-type Si-microprobe array by selective vapor–liquid–solid (VLS) growth method *Japan. J. Appl. Phys.* **44** 2161–5
[16] Hirayama H, Tatsumi T and Aizaki N 1988 Selective growth condition in disilane gas source silicon molecular beam epitaxy *Appl. Phys. Lett.* **52** 2242–3
[17] Matsuda K, Suzuki K, Yamamura K and Kanda Y 1993 Nonlinear piezoresistance effects in silicon *J. Appl. Phys.* **73** 1838–47
[18] Sze S M 1981 *Physics of Semiconductor Devices* 2nd edn (New York: Wiley)
[19] Middelhoek S and Audet S A 1989 *Silicon Sensors* (London: Academic)